A SKY SURVEY OF NEUTRAL HYDROGEN AT λ 21 CM

III. GAS AT HIGHER RADIAL VELOCITIES

By R. X. McGee* and Janice A. Milton*

[*Manuscript received September* 18, 1963]

Summary

Information is presented concerning the distributions of the intensity and radial velocity of atomic hydrogen gas at radial velocities away from zero. The observations were made with an aerial beam of 2°.2 between half-power points and a multichannel H-line receiver of channel spacing equivalent to 7 km/s and bandwidth 38 kc/s ($\approx$ 8 km/s).

The gas at the higher velocities is found in the galactic latitude range $b^{\mathrm{II}} = \pm 10°$ arrayed in a number of spiral arms. The simply reduced observational data are compared with the refined reductions of previous workers in the case of the outer ($R > R_0$) arms.

It is shown that, if use is made of the radial velocity–distance models at present accepted, the principal elements of the gaseous spiral arms are clouds of enormous size. The size of the clouds and hence the thickness of the spiral arms apparently increases markedly with distance from the galactic centre greater than solar distance (R_0). The masses of these large clouds remain fairly uniform at $\sim 10^7 \mathrm{M}_\odot$.

I. Introduction

Galactic neutral hydrogen at other than small radial velocities is, in general, confined to the Milky Way regions and is observed between galactic latitudes $b^{\mathrm{II}} = \pm 10°$. The low velocity gas discussed in paper II (McGee, Murray, and Milton 1963) is concentrated to the galactic plane but appears at all latitudes because of its local nature. The distribution of atomic hydrogen in the Milky Way has been subjected to intensive study and discussion by the workers in two observatories particularly: Leiden (van de Hulst, Muller, and Oort 1954; Muller and Westerhout 1957; Ollongren and van de Hulst 1957; Schmidt 1957) and the Radiophysics Laboratory, Sydney (Kerr, Hindman, and Gum 1959).

Using similar reduction and analytical techniques they have produced the picture of the spiral structure of our Galaxy accepted at present. The work on the inner parts, i.e. those at distances less than the Sun–galactic centre distance, has been mainly responsible for the establishment of the new IAU System of Galactic Coordinates (Blaauw *et al.* 1960).

This paper aims to show how the higher velocity atomic hydrogen appears to the observer before any great amount of reduction, correction, and analysis is applied. Attention is directed to the gas in the outer parts of the Galaxy where it is shown that the spiral arms appear to consist of extremely large complexes whose dimensions increase and densities decrease with distance from the galactic centre.

The results have emerged incidentally from the sky survey carried out at Murraybank, Sydney, which was directed primarily towards mapping the local

* Division of Radiophysics, CSIRO, University Grounds, Chippendale, N.S.W.

hydrogen. The aerial beam used had a half-power beam width of 2°.2. The receiver was the 48 channel H-line instrument of bandwidth 38 kc/s, and channel spacing equivalent to 7 km/s in radial velocity. The apparatus and the local gas have been discussed by McGee and Murray (1961, 1963) and McGee, Murray, and Milton (1963).

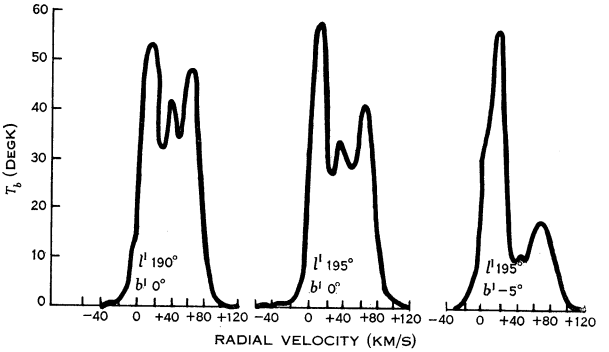

Fig. 1.—Typical triple-peaked hydrogen line profiles to illustrate the grouping of intensity data into certain radial velocity ranges.

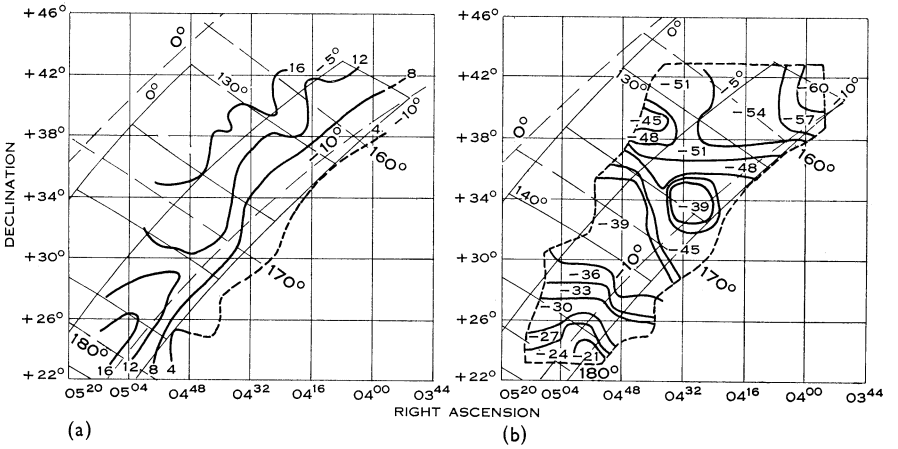

Fig. 2

Figs. 2(*a*) to 14(*a*).—Intensity contours of neutral hydrogen in terms of $T_{\text{max.}}$, the temperature at an H-line profile peak. The contour interval is 4°K. Coordinates: equatorial (1960); l^{I}, b^{I} (old galactic), full line; l^{II}, b^{II} (new galactic), broken line. The sequence is that galactic longitude increases from $l^{\text{II}} = 160°$ in Figure 2 to $l^{\text{II}} = 50°$ in Figure 14. The l^{II} ranges for each diagram are given in Table 1 (p. 148).

Figs. 2(*b*) to 14(*b*).—Companion diagrams to Figures 2(*a*) to 14(*a*). Contours, at intervals of 3 km/s, of radial velocity of neutral hydrogen at the H-line profile peak. Values refer to velocities in the areas between contours. Each diagram is complementary to the intensity diagram of the corresponding number.

II. Presentation of the Data

Following the procedure of paper II we again represent the neutral hydrogen intensity in terms of the $T_{\text{max.}}$, the brightness temperature at an H-line profile peak. The radial velocity information is given as the values at the $T_{\text{max.}}$ points.

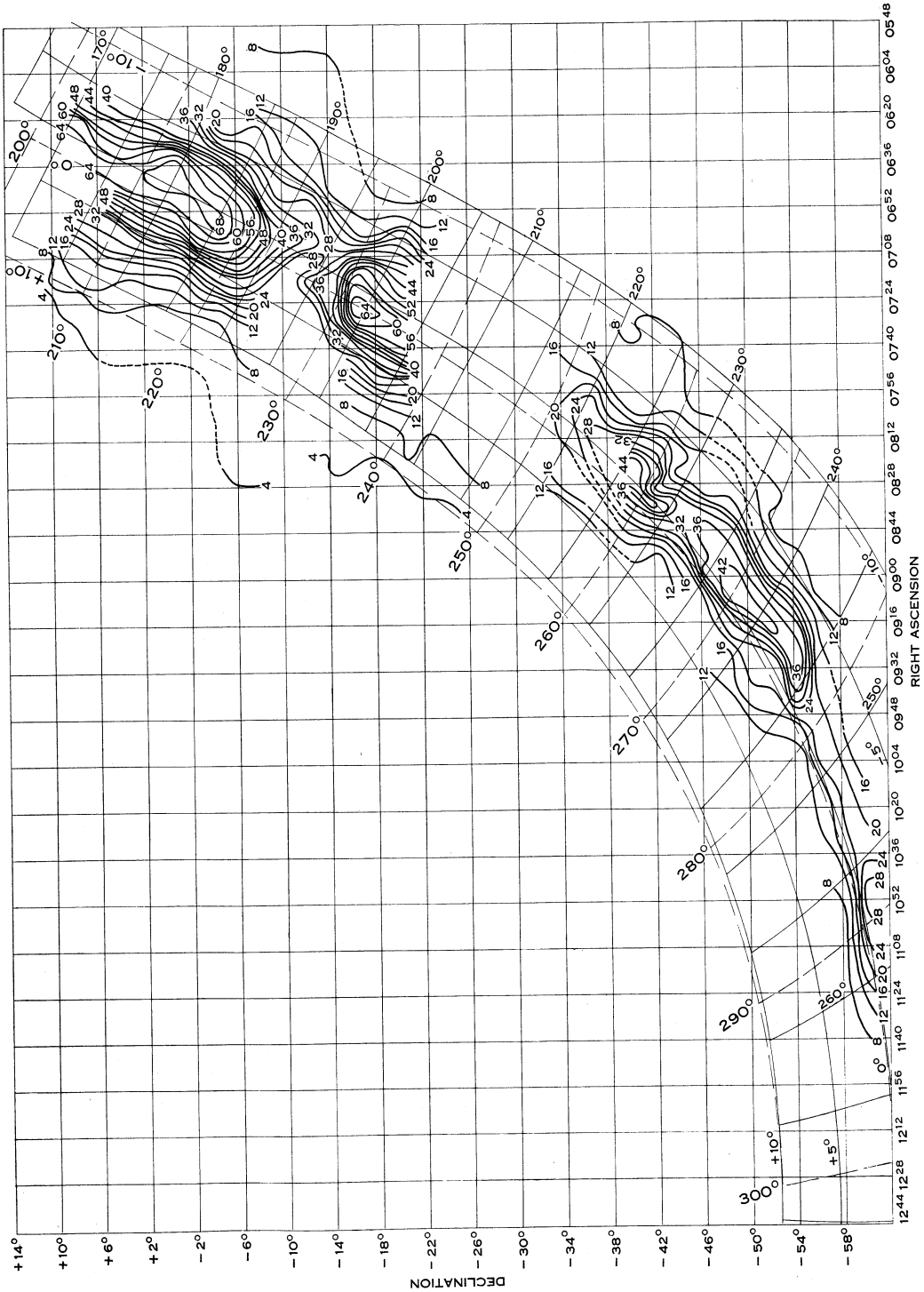

Fig. 3(*a*)

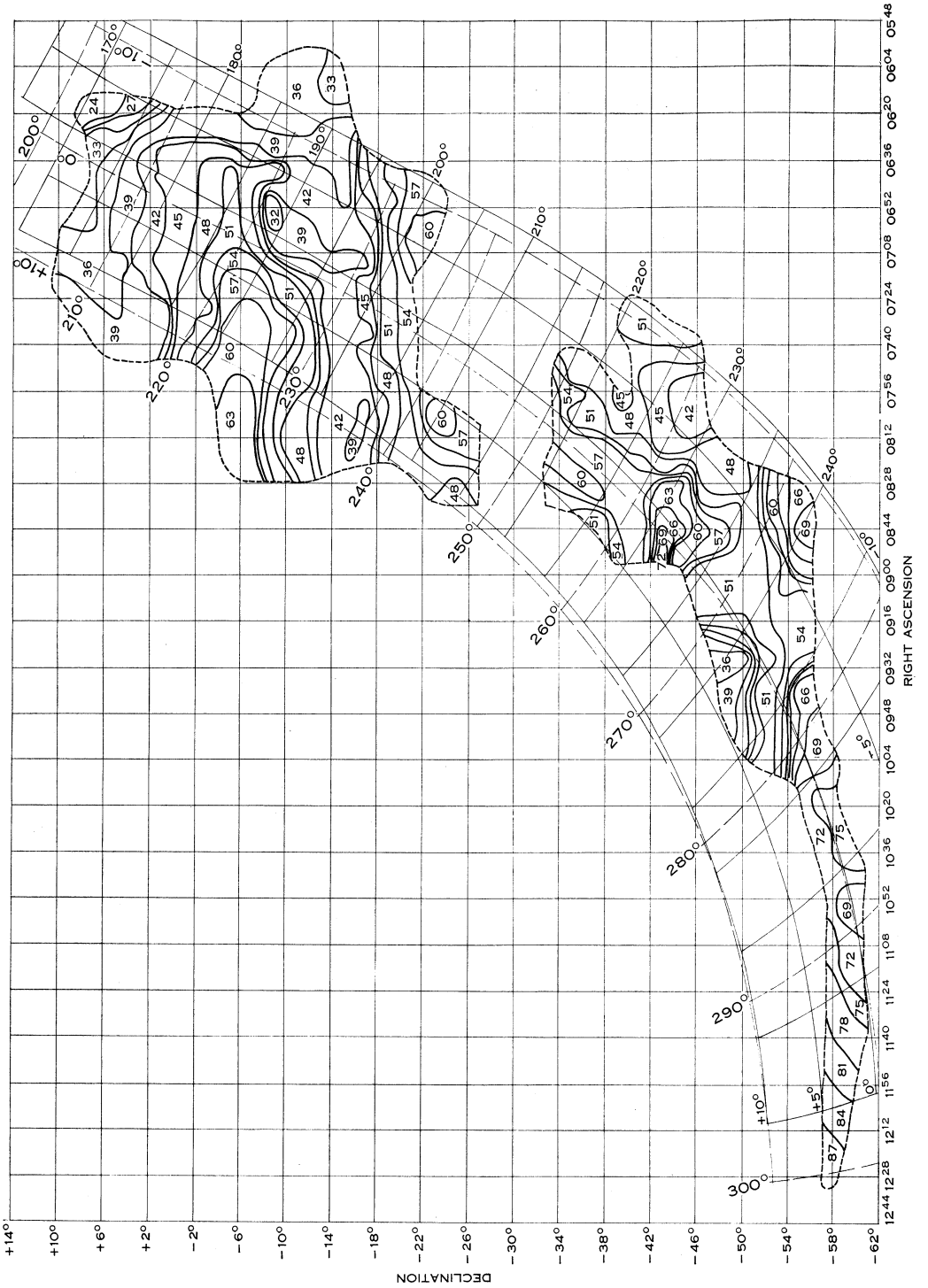

Fig. 3(b)

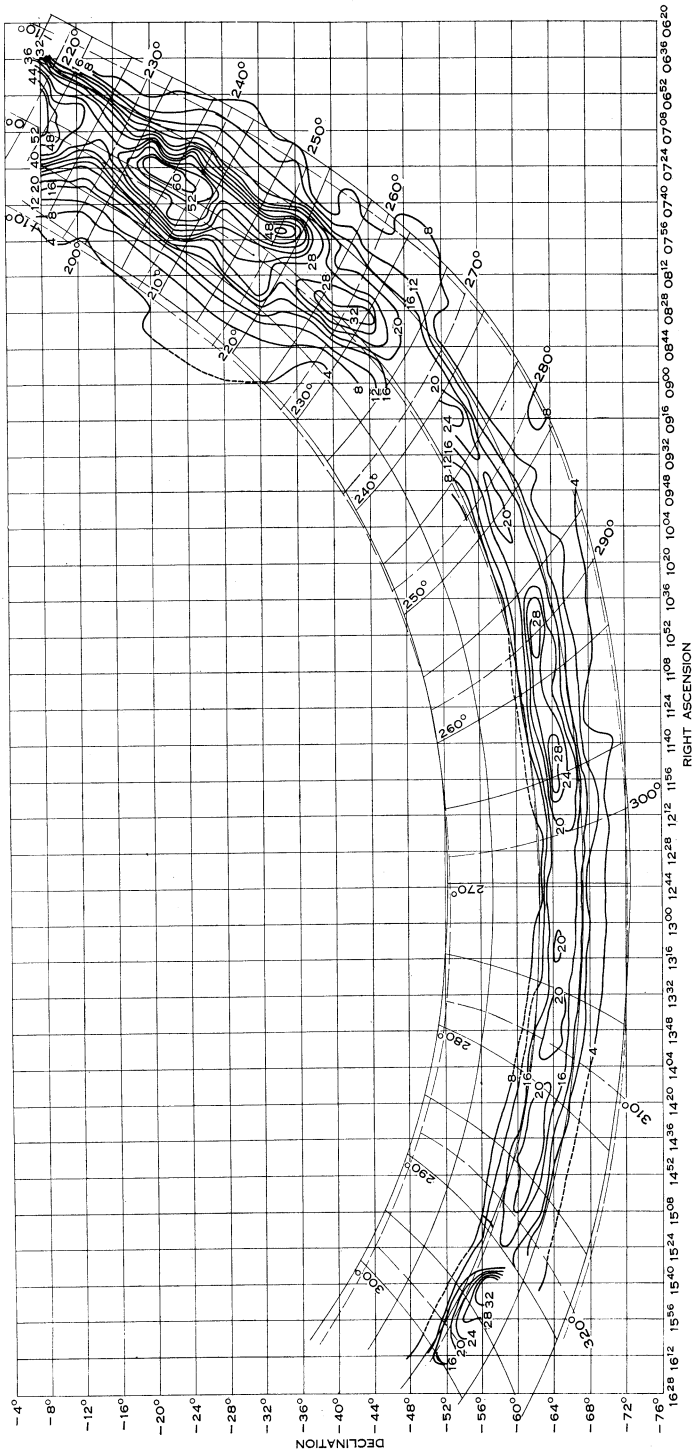

Fig. 4(*a*)

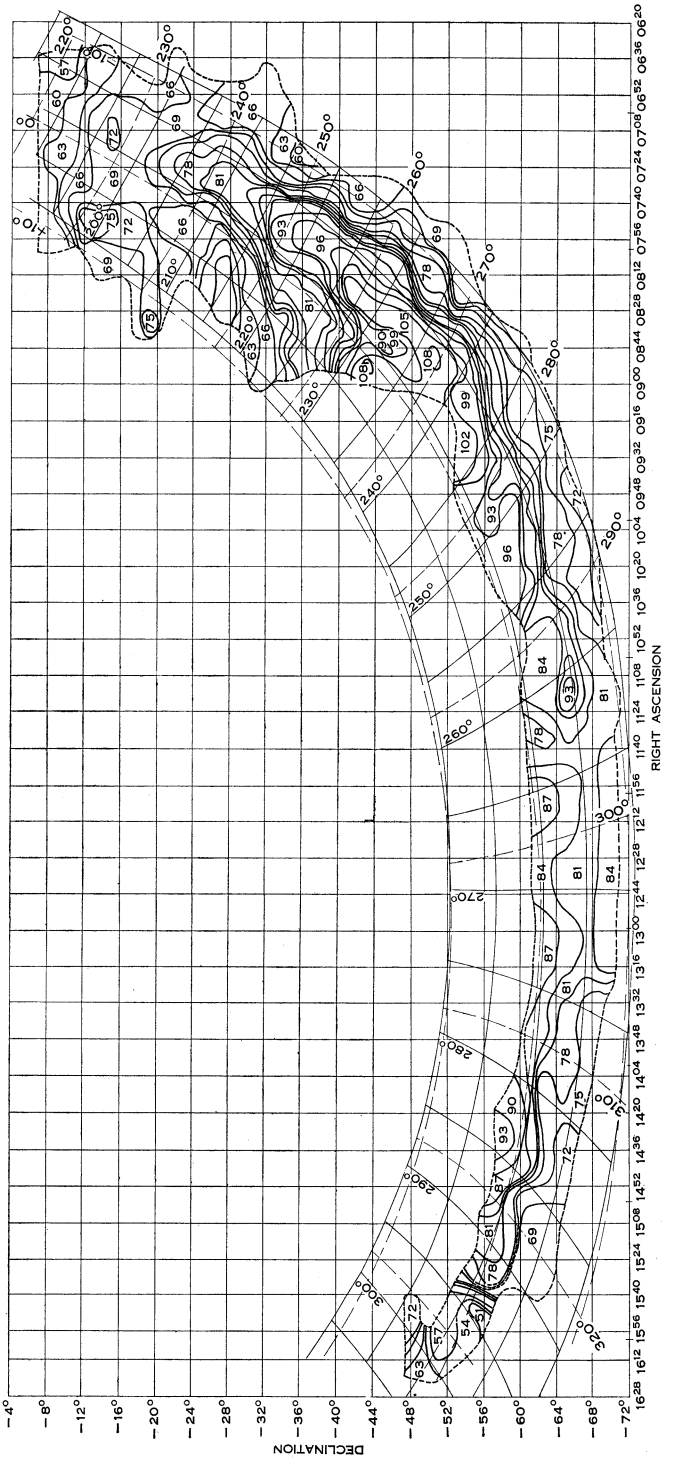

Fig. 4(b)

The velocities are referred to the local standard of rest with the aid of tables prepared by MacRae and Westerhout (1956).

The first step in presenting the observations is to decide on the grouping of intensities in certain velocity ranges. The method used is, perhaps, best explained by an example. Three triple-peaked profiles are shown in Figure 1. The central profile at $l^{\mathrm{I}} = 195°$, $b^{\mathrm{I}} = 0°$ has peaks with radial velocities +13, +36, and +67 km/s. The profile on the left is 5° removed in galactic longitude but at the same latitude; peaks occur at velocities +12, +35, and +62 km/s. The profile on the right is 5° away in latitude but at the same longitude as the central one; peaks are at +15, +44 (almost disappeared), and +68 km/s. The peak velocities and shape change slowly with position and these three peaks in distinct velocity ranges can clearly be

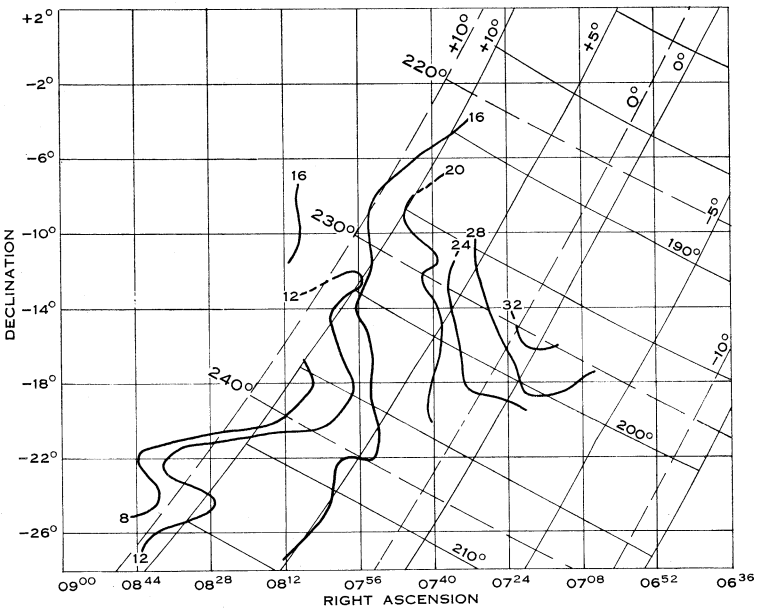

Fig. 5(*a*)

distinguished as separate physical entities. When many profiles at quite close spacing are available peaks in similar velocity ranges may be followed across and along the galactic plane in the form of contour diagrams of $T_{\mathrm{max.}}$ and companion diagrams of contours of the radial velocities at $T_{\mathrm{max.}}$. In the sky survey profiles were observed at intervals of 2 min in right ascension and 1° in declination. $T_{\mathrm{max.}}$ and radial velocity data have been plotted whenever peaks could be distinguished. No attempt was made to follow a particular peak if its characteristic velocity was submerged in the side of a nearby (in radial velocity), more intense peak. For example, in Figure 3, no contours have been drawn in the confused region between declinations −23° and −32° approximately.

Thirteen pairs of contour diagrams of $T_{\mathrm{max.}}$ and of radial velocities at $T_{\mathrm{max.}}$ are given in Figures 2 to 14. The galactic longitude range (l^{II}) for each is listed in Table 1 (see p. 148). In some cases the information extends over only 20°

in longitude, in others over more than 100°. The sequence of diagrams is such that $l^{II} = 160°$ occurs in Figure 2, $l^{II} = 0°$ in Figure 10, and $l^{II} = 50°$ in Figure 14. The intensity distributions, $T_{max.}$, are contained in the thirteen (*a*) diagrams while the companion radial velocity distributions are found in the (*b*) diagrams.

An equatorial coordinates grid has been used with declinations marked every 4° and right ascension every 16 min. Old galactic coordinates (l^{I}, b^{I}) are superimposed in 5° intervals, new galactic coordinates (l^{II}, b^{II}) in 10° intervals. The $T_{max.}$ contour interval is 4°K. The radial velocities have been treated as in paper II, i.e. running averages of six or more readings were taken over areas 2° square and areas of radial velocity in ranges of 3 km/s are enclosed by contour lines.

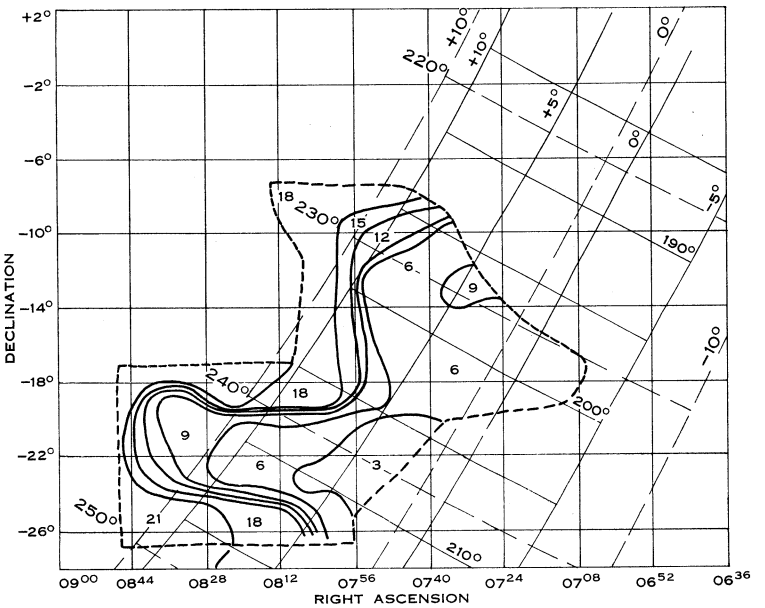

Fig. 5(*b*)

The contours of $T_{max.}$ in Figures 2(*a*) and 5(*a*) have no particular form but all the remaining sets have a characteristic shape. They appear to depict the gaseous spiral arms along and perpendicular to the galactic plane. In general, the latitude spread is seldom more than ±10°, the minimum extent observed in latitude has a half-power width of about $3\frac{1}{2}°$. A number of maxima, apparently representing concentrations of gas, occur in each diagram centred on latitudes up to $b^{II} = +2\frac{1}{2}°$ in "northern" longitudes to $b^{II} = -3\frac{1}{2}°$ in "southern" longitudes. ($l^{II} \approx 200°$ to 350°.)

It is possible to obtain an estimate for N_H, the number of hydrogen atoms per cm² in a line-of-sight column to within ±30% by using the simple relation:

$$N_H = 6 \times 10^{19}\, T_{max.}. \tag{1}$$

The constant term is the gradient of a mean curve through some 3000 points of an N_H versus $T_{max.}$ diagram. The single-peaked profiles from which this information was

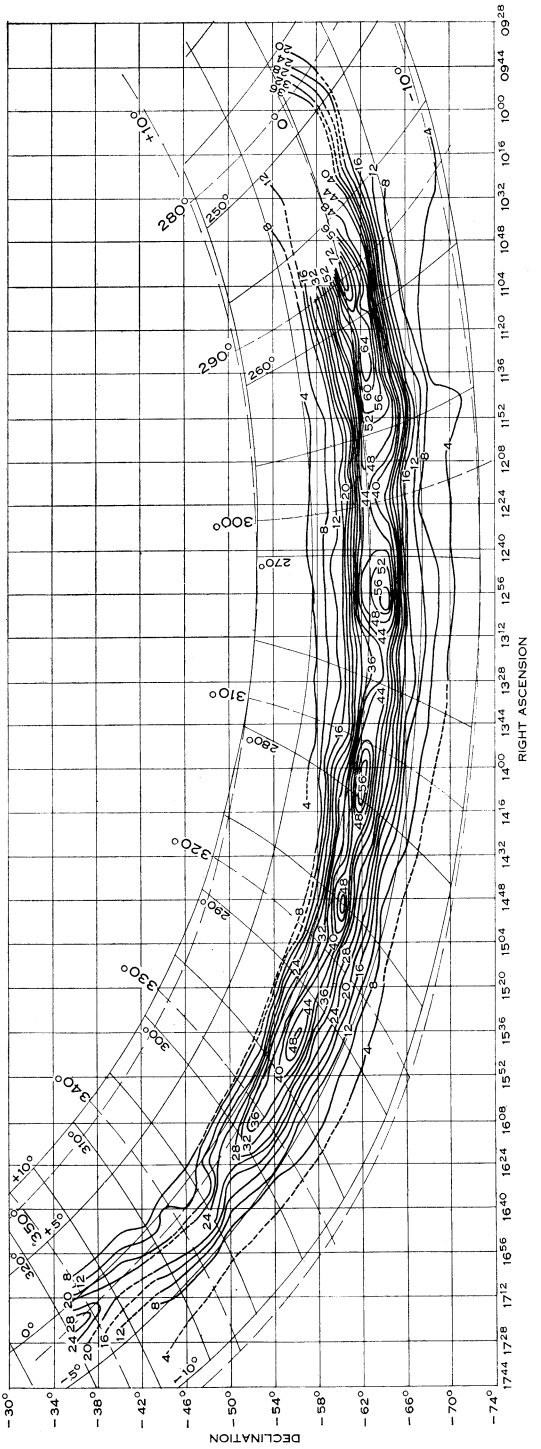

Fig. 6(*a*)

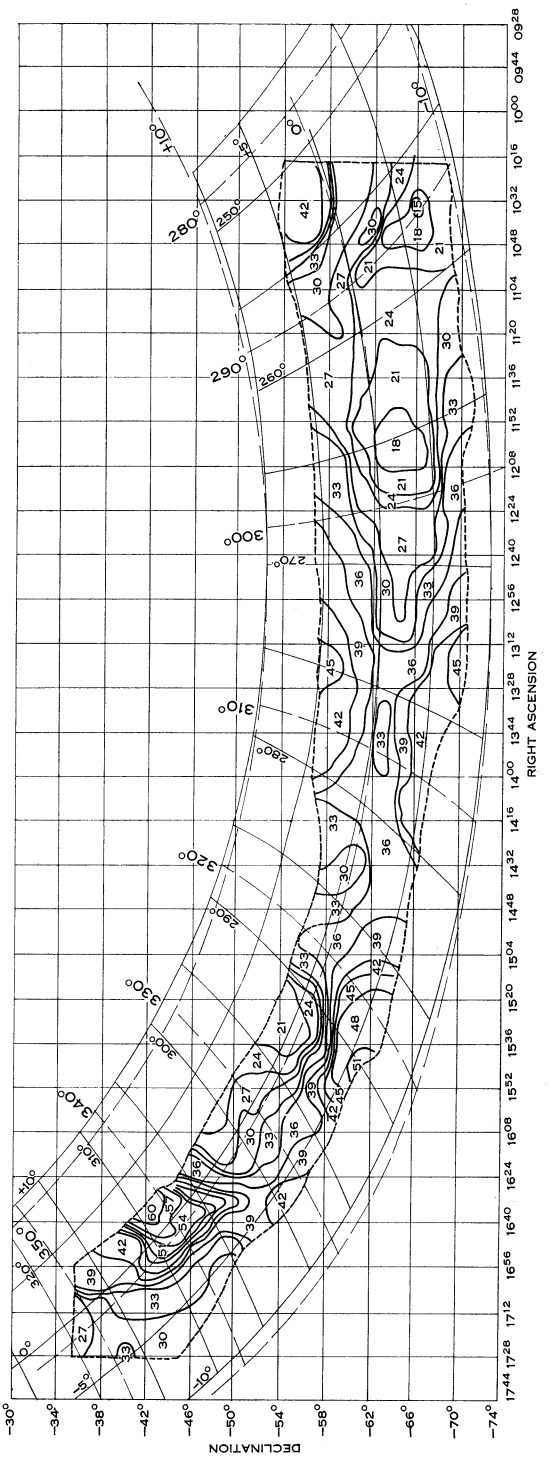

Fig. 6(*b*)

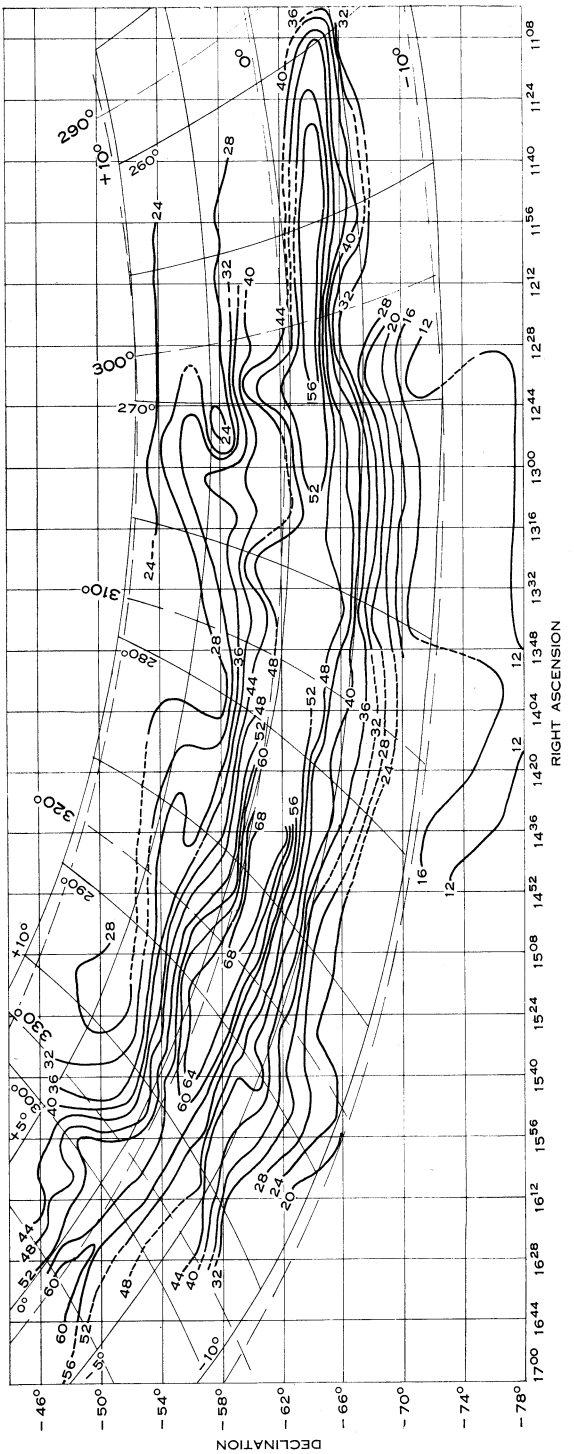

Fig. 7(a)

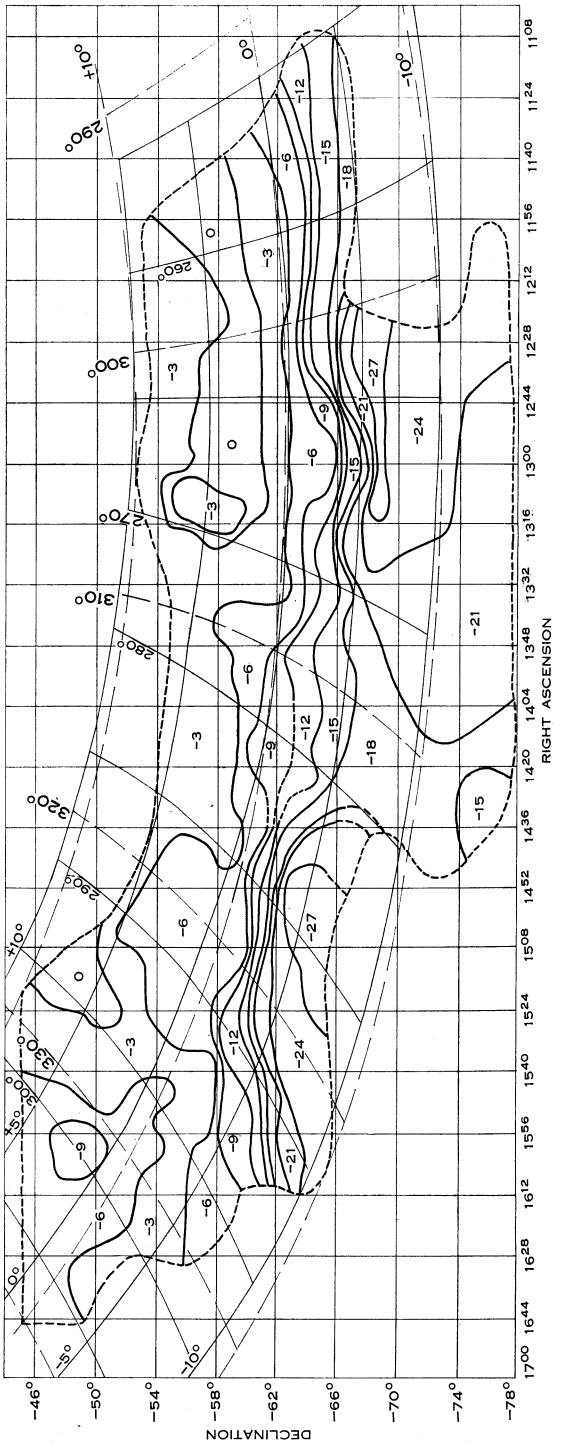
RIGHT ASCENSION
DECLINATION
11⁰⁸
11²⁴
11⁴⁰
11⁵⁶
12¹²
12²⁸
12⁴⁴
13⁰⁰
13¹⁶
13³²
13⁴⁸
14⁰⁴
14²⁰
14³⁶
14⁵²
15⁰⁸
15²⁴
15⁴⁰
15⁵⁶
16¹²
16²⁸
16⁴⁴
17⁰⁰
−46°
−50°
−54°
−58°
−62°
−66°
−70°
−74°
−78°
+10°
+5°
0°
−5°
−10°
290°
300°
310°
320°
330°
280°
270°
260°

Fig. 7(b)

gathered were chosen at random but in ranges to represent all galactic latitudes. However, the gas was, in general, confined to the solar vicinity. We assume that the same relation will apply in other galactic spiral arms.

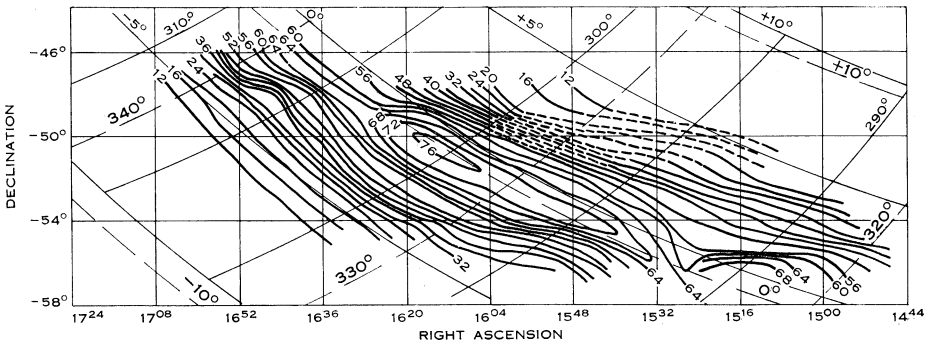

Fig. 8(*a*)

The velocity contours of Figure 7 are in a rather low negative range (average along the ridge is about -5 km/s) and the corresponding $T_{\max.}$ contours contain a number of discontinuities. This is the region where a higher negative velocity range was chosen for the "low velocity" gas, for reasons discussed in paper II.

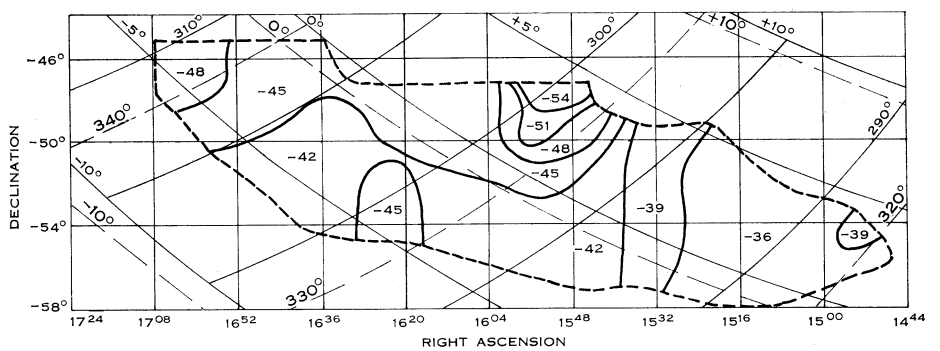

Fig. 8(*b*)

III. Comparison with Previous Work

In making a comparison with previous work it is necessary to invoke a radial velocity-distance model, such as those used to reduce the Leiden and Potts Hill, Sydney, observations. We have chosen the model suggested by Kerr (1962), in which he has adjusted both the northern and southern sets of data to include the galactic rotation and an expansion component.

From the radial velocity–distance–galactic longitude diagram for $b^{\mathrm{II}} = 0°$ (see Fig. 7 in Kerr 1962) it is possible in some cases to decide at what distance the intensity contours should be considered: Figures 7, 8, 9, 10, 11, 12, and 14 apply to regions at distances from the galactic centre less than the Sun's distance, $R < R_0$.

An ambiguity of position exists and so no general comparison has been thought worth while. Some individual HI concentrations in these regions are discussed later. Figures 2, 3, 4, 5, 6, and 13 have $R > R_0$ and are easily fitted into the distance diagram: the positions of the central ridges of neutral hydrogen, as delineated in

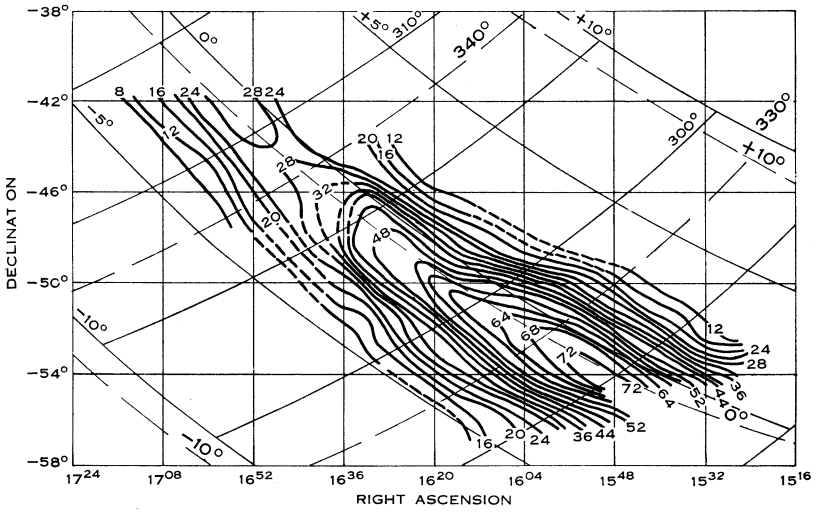

Fig. 9(*a*)

the $T_{\max.}$ contours of Figures 3, 4, 6, and 13, have been superimposed on the corresponding "outer parts" of the HI density distribution in the galactic plane (from

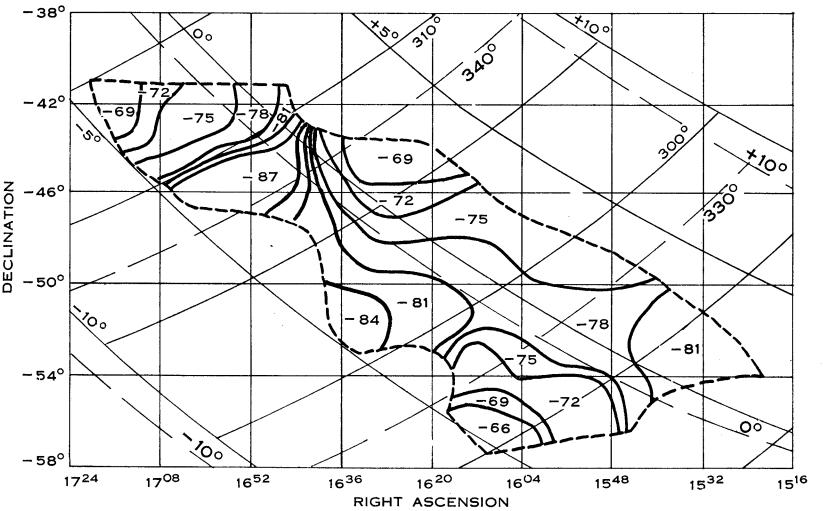

Fig. 9(*b*)

Fig. 9 of Kerr 1962). In Figure 15 the circles mark the positions of the maxima of the hydrogen concentrations, the crosses the positions of the minimum intensities on the ridges projected onto the plane $b^{\mathrm{II}} = 0$.

We see in Figure 15 the central line of four outer gaseous arms as revealed directly from observations compared with the distribution of HI derived from greatly refined reductions. A general agreement may be noted. In a number of cases corres-

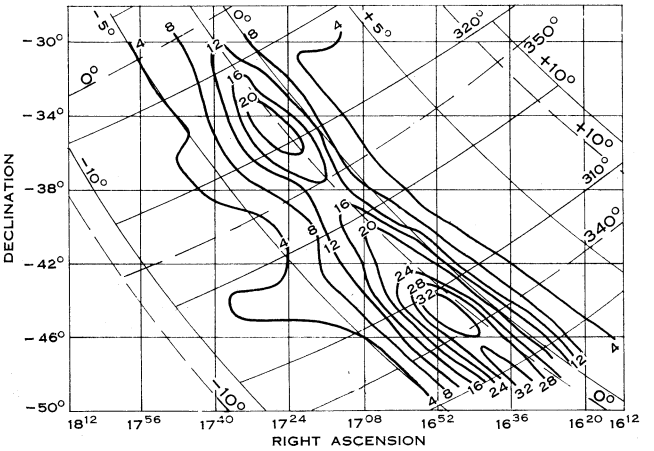

Fig. 10(*a*)

pondences occur between HI concentrations and regions of increased density and between HI deficiencies and regions of comparatively lower density.

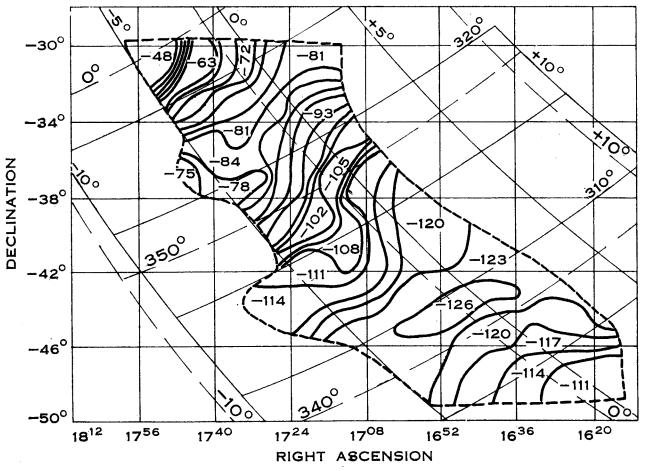

Fig. 10(*b*)

IV. Concentrations of Neutral Hydrogen

Although it is generally admitted that the radial velocity conditions in the outer parts of our Galaxy are not well known, the disposition of neutral hydrogen as seen in Figure 15 provides at least a reasonable working basis. Estimates of sizes and densities of the HI concentrations are thus possible.

HI concentrations are recognized in the disposition of the $T_{\max.}$ contours. In Figure 3, for example, we may see the contour pattern rise up to a maximum near $l^{\mathrm{II}} \sim 215°$, $b^{\mathrm{II}} \sim -1\overset{\circ}{.}5$ and, again, near $l^{\mathrm{II}} \sim 232°$, $b^{\mathrm{II}} \sim 0°$. Their shapes give the impression of clouds or complexes of gas. The same pattern is seen throughout most of the contour diagrams. Further indirect evidence of single entities from the radial velocity distributions is discussed in the next section.

The thickness of a cloud has been measured as that between half-intensity levels. Some previous information, such as the thickness of the HI gas layer, has been quoted at the half-density points (Schmidt 1957), for which a knowledge of the spin temperature is required. However, recent observations, especially with the 210-ft aerial, have produced temperatures far in excess of the previously assumed constant value of 125°K. Thus, until this point is clarified and if we take into account the fact that most of the $T_{\max.}$ maximum temperatures are no greater than 70°K, the half-intensity thickness is considered a preferable quantity.

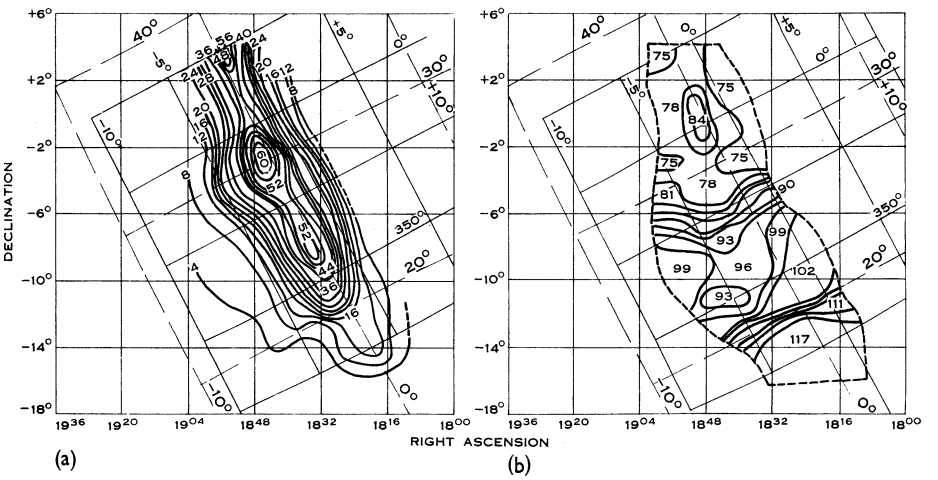

Fig. 11

The usual simple aerial beam corrections (e.g. Bracewell and Roberts 1954) were applied to the estimated angular dimensions of the HI concentrations. Distance from the Sun, from the radial–velocity–distance model, enabled linear dimensions to be assigned to the l and b coordinates. Further assumptions—(*a*) that the shape of the contributing H-line at the radial velocity of the concentration (i.e. using equation (1)) and (*b*) that the thickness of the concentration in the galactic plane is equal to the extent in latitude (a cylindrical shape for these large components of spiral arms would seem the most reasonable)—lead to an estimate of $\bar{n}_{\mathrm{H}}$, the average gas density in atoms cm^{-3}.

These particulars, together with the galactic and equatorial coordinates, the values of $T_{\max.}$, and radial velocities (r.v.) at the maximum intensities of the concentrations, are in Table 2 (p. 150). The scatter ($\Delta_{\mathrm{r.v.}}$), defined as the difference between the highest and lowest values of radial velocities within the apparent

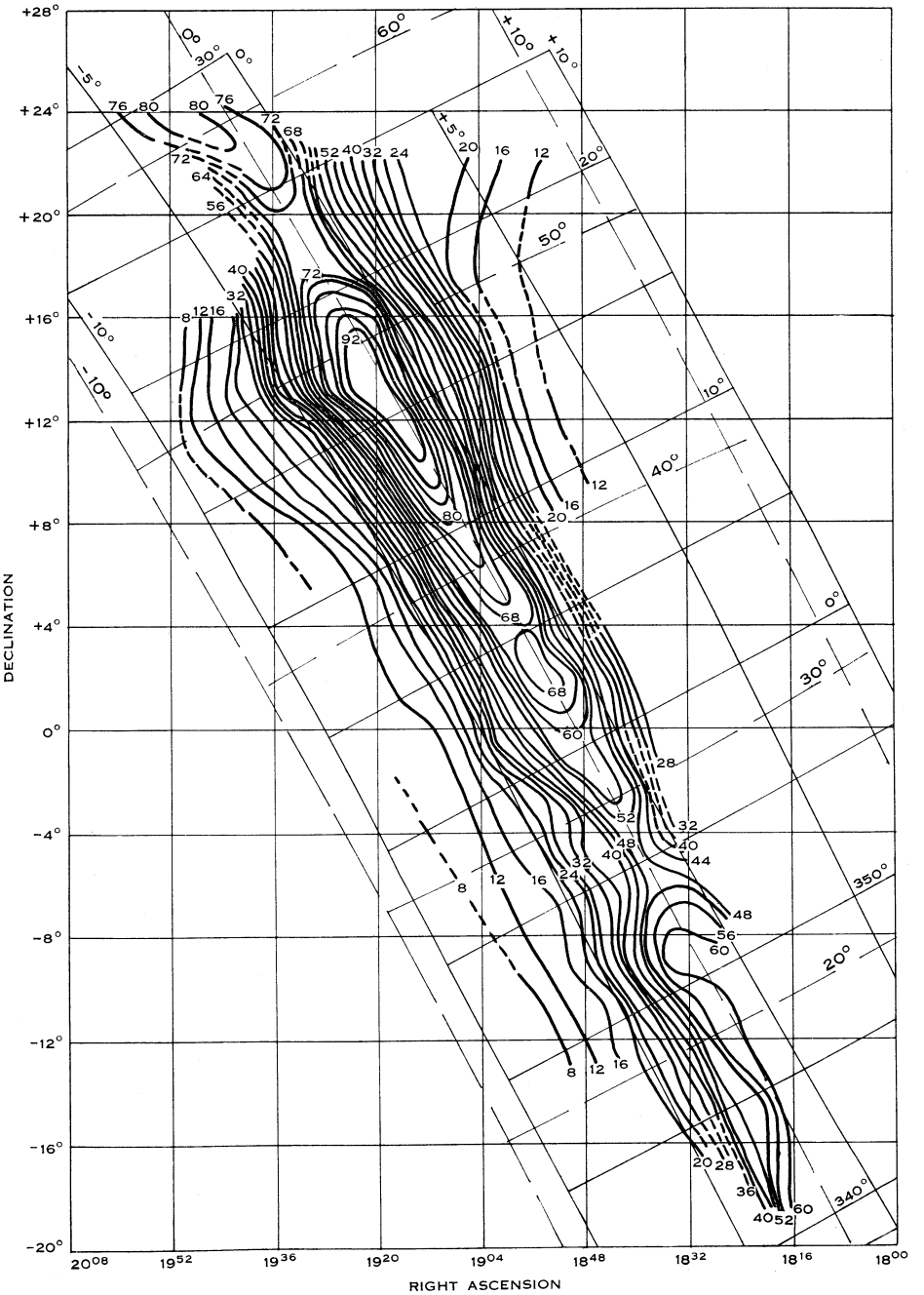
DECLINATION
RIGHT ASCENSION
+28°
+24°
+20°
+16°
+12°
+8°
+4°
0°
-4°
-8°
-12°
-16°
-20°
20^08
19^52
19^36
19^20
19^04
18^48
18^32
18^16
18^00
60°
50°
40°
30°
20°
10°
0°
350°
340°
+10°
+5°
-5°
-10°

Fig. 12(*a*)

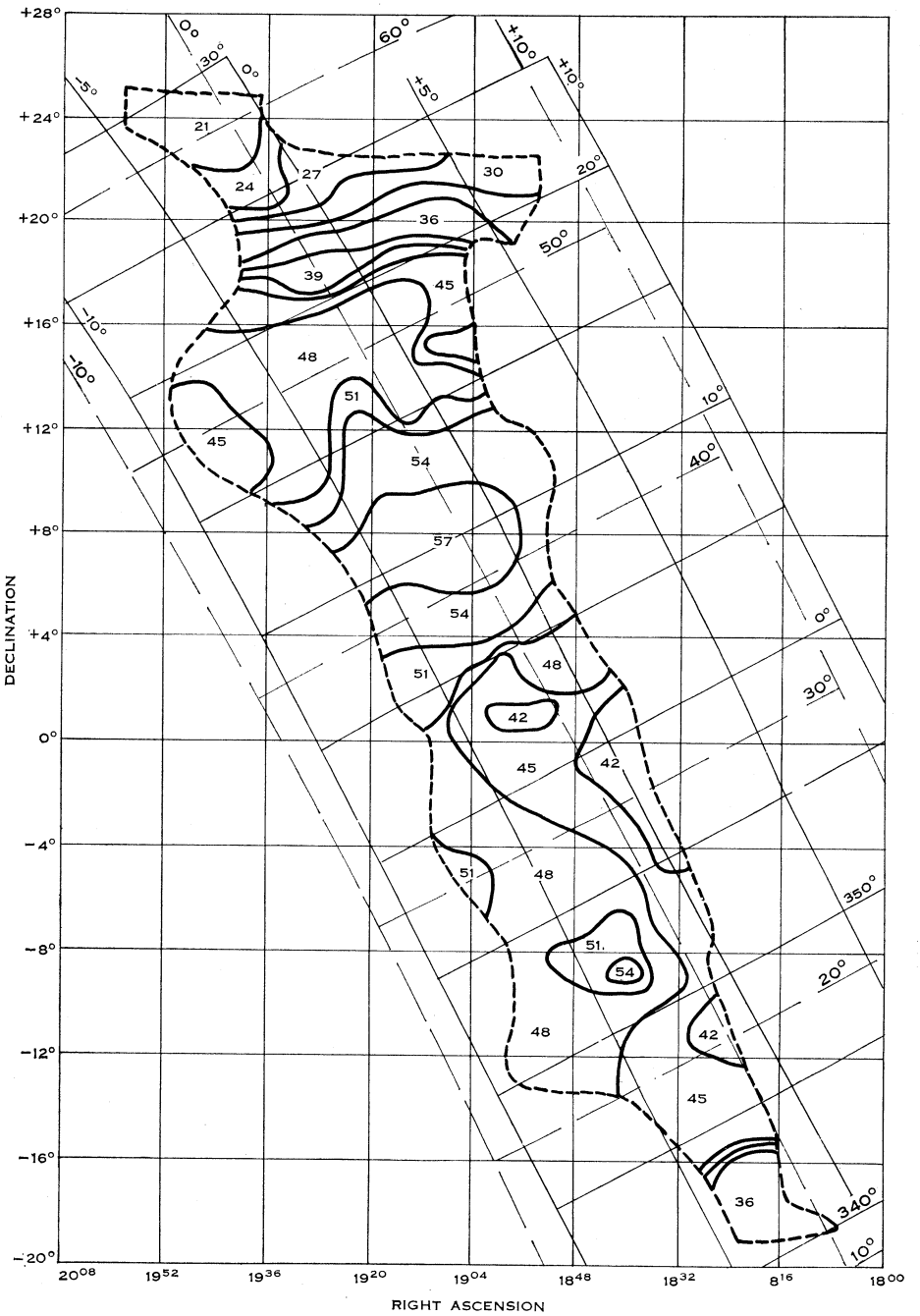
DECLINATION
RIGHT ASCENSION
+28°
+24°
+20°
+16°
+12°
+8°
+4°
0°
-4°
-8°
-12°
-16°
-20°
20h08
19h52
19h36
19h20
19h04
18h48
18h32
8h16
18h00
21
24
27
30
36
39
45
48
51
54
57
42
0°
30°
60°
-5°
+5°
+10°
20°
50°
-10°
10°
40°
350°
340°

Fig. 12(*b*)

boundaries of an HI concentration, the distances from the galactic centre, and the numbers of the figures where the concentrations occur, are given. Part A of the table refers to concentrations at distances $R > R_0$ and contains additional information, on the half-power aerial resolution in terms of linear dimensions in parsecs and the

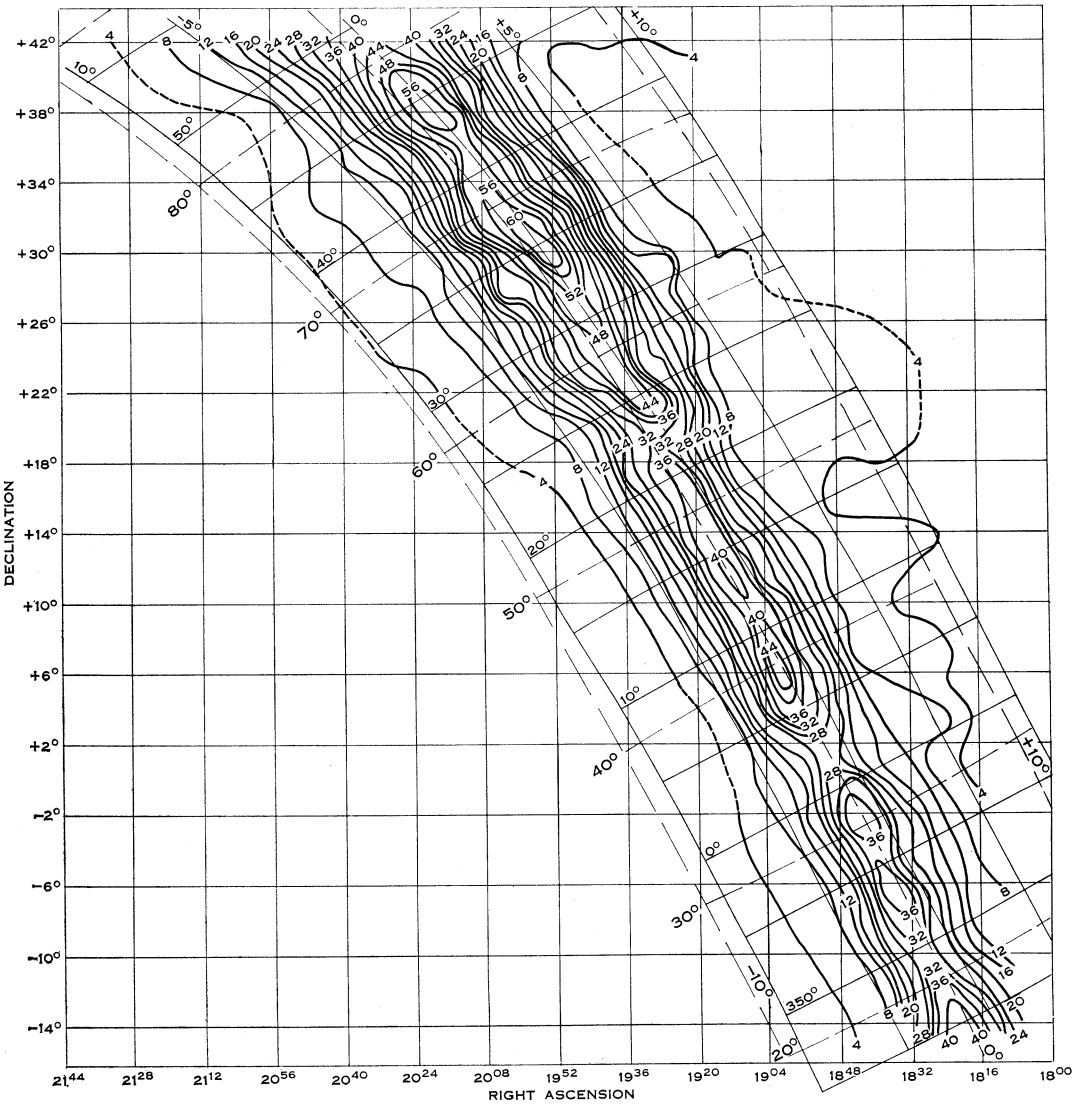

Fig. 13(*a*)

deviation of the cloud centres from the galactic plane. The deviation or distortion of the gas layer out of the galactic plane has been discussed by Kerr (1962). Part B refers to distances $R < R_0$. Here the model introduces an ambiguity in distance and two sets of dimensions and average densities are given for most entries.

(*a*) *HI Clouds at* $R > R_0$

Before discussing the data revealed in Table 2 we review some of the knowledge on sizes of the larger interstellar gas clouds. Van de Hulst (1958) has published a

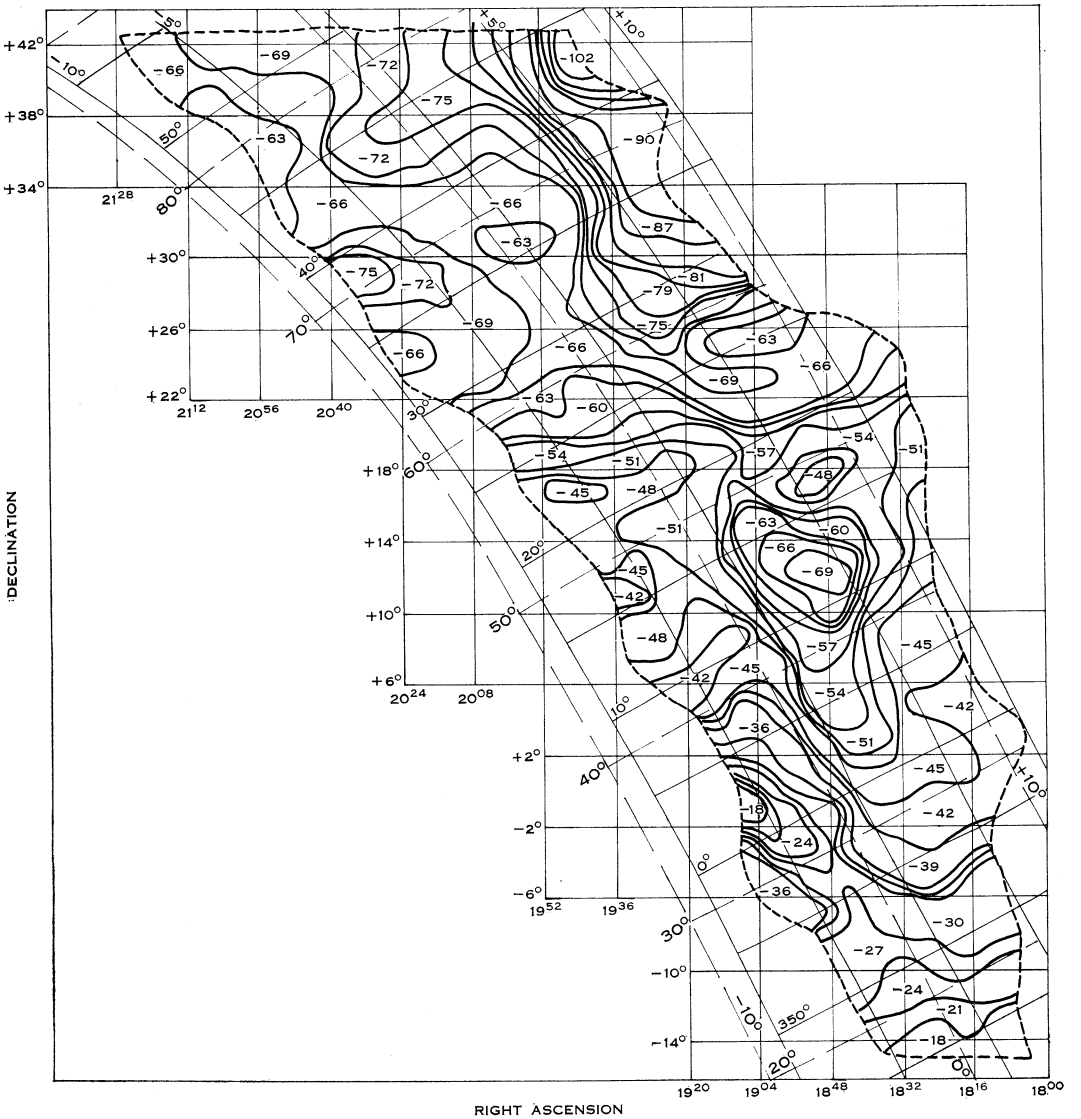

Fig. 13(*b*)

table summarizing estimates of cloud size. Of interest here are the following entries:

Diameter of spiral arm in plane	500–1000 pc
Diameter of spiral arm ⊥ plane	200
Condensations in spiral arm	100

Large emission region	60
Typical cloud, Ca^+ absorption	30
Typical cloud, 21 cm emission	20 – 70

One of us (McGee 1963) has drawn attention to the existence of two further classes of HI concentrations. The first, of dimensions 100–150 parsecs, containing two or more of van de Hulst's "typical clouds, 21 cm emission" has been observed in the solar vicinity. Further details are included in paper II (McGee, Murray, and Milton 1963).

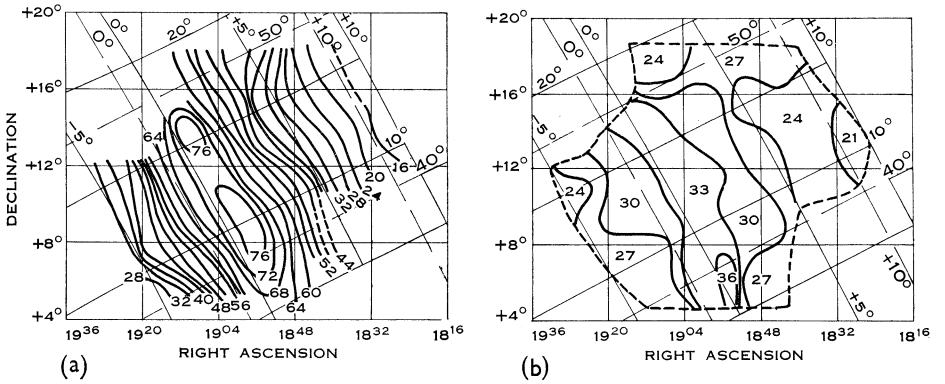

Fig. 14

HI clouds of the second class are several times larger and are found in the regions of $R > R_0$. Part A of Table 2 contains 29 examples with latitude- or z-dimensions in the range 350–1330 parsecs. This dimension is easily obtained from

TABLE 1

RANGE OF GALACTIC LONGITUDE (l^{II}) FOR FIGURES 2 TO 14

l^{II} Range	Fig. No.	l^{II} Range	Fig. No.
160°–180°	2	325°–345°	9
200°–295°	3	335°– 0°	10
220°–330°	4	15°– 35°	11
225°–245°	5	15°– 60°	12
280°–350°	6	15°– 85°	13
290°–340°	7	35°– 50°	14
320°–340°	8		

the contour diagrams but must be regarded as approximate only. Although aerial beam corrections for smoothing have been applied, recent experience of observations with 10 times better resolution (14′) indicate that such corrections are only approximate to the true distributions in many cases. However, the equivalent aerial resolution dimensions (column 14) indicate that a good margin nearly always exists between the b value and the resolution limit.

The dimension in longitude has been estimated rather than measured from the contour diagrams, and in 10 of the Table 2A examples two or three maxima occur at such spacing that only one overall l-dimension can be estimated. The average l/b ratio is about 2·7.

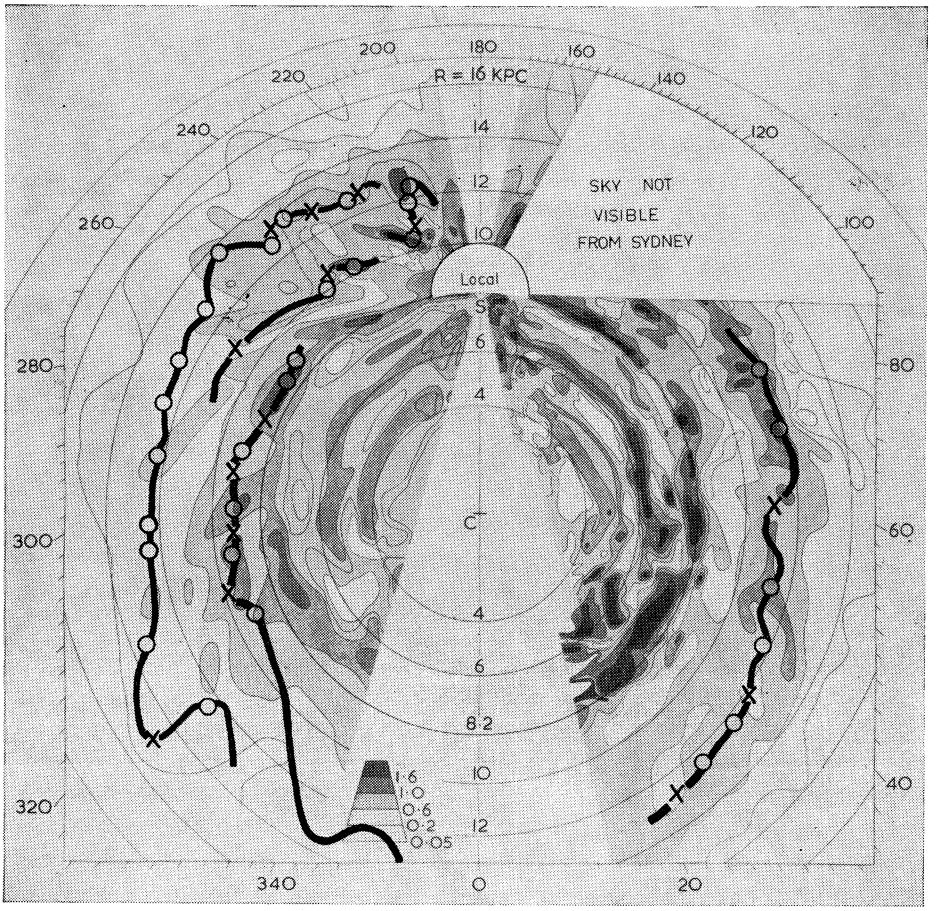

Fig. 15.—The ridges of maximum intensity of four spiral arms, at $R > R_0$, of neutral hydrogen (represented by heavy lines) superimposed on the outer parts of Kerr's "distribution of neutral hydrogen in the Galaxy (unit = atom/cm³) based on a model involving both rotation and expansion". The circles are the positions of maximum intensity of concentrations, the crosses the position of minimum intensity between concentrations.

The masses of these large complexes are all of the same order, with an average value from calculations on nine of the clouds of $10^7 M_\odot$.

The deviations from the plane $b^{II} = 0$, seen in column 17 of Table 2A, have been calculated from the b^{II} values at the maximum intensities in concentrations. The trends for deviations, negative on the $l^{II} = 200°$ to $350°$ side and positive at $l^{II} = 20°$ to $80°$, are the same as previously reported (e.g. Kerr 1962) but individual values do not fit very well into Kerr's contours. $\Delta_{r.v.}$, the scatter of radial velocity,

TABLE 2

CONCENTRATIONS OF NEUTRAL HYDROGEN NEAR THE GALACTIC PLANE

A. At distances $R > R_0$

No.	l^{II} (deg)	b^{II} (deg)	α_{1960} h	α_{1960} m	δ_{1960} (deg)	$T_{max.}$ (°K)	r.v. (km/s)	$\Delta_{r.v.}$ (km/s)	Corrected Angular Dimensions b (deg)	Corrected Angular Dimensions l (deg)	r (kpc)	Linear Dimensions b (pc)	Linear Dimensions l (pc)	Equiv. Res. to ½-power	R (kpc)	$\bar{n}_H$ (H atoms cm^{-3})	Deviations (pc)	Fig. No.
1.a	212·2	−2·1	06	40	− 0·2	68	+ 45	17	8·5	18	4	590	1250	150	12	1·1	−385	3
1.b	217·4	−0·8	06	54	− 4·3	68	+ 48										−147	3
2	232·2	+0·1	07	26	−16·9	64	+ 45	12	6·7	13	3	350	680	120	10·2	1·8	+ 18	3
3	236·6	−2·2	07	26	−21·9	60	+ 75	12	8·5	17	6	890	1750	230	12·5	0·7	−480	4
4	250·2	−3·5	07	52	−34·3	52	+ 93	12	8·4	12	7·8	1145	1650	300	13	0·5	−764	4
5.a	257·8	−0·5	08	25	−39·1	32	+ 87	24	6·2	15	9	970	2350	350	13	0·3	−109	4
5.b	261·5	−2·0	08	30	−42·9	32	+100										−436	4
6	258·9	−1·6	08	25	−40·3	44	+ 57	9	6·2	13	5	540	1150	190	10·2	0·8	−293	3
7	270·0	−1·1	09	05	−48·9	42	+ 51	15	5	16·5	6	520	1750	230	10	0·8	−201	3
8.a	273·7	−3·2	09	12	−53·0	24	+ 99	12	3	16	10·7	555	3100	410	12·8	0·4	−699	4
8.b	281·8	−2·9	09	56	−58·2	20	+ 96	18	4		11·7	820		450	12·5	0·3	−632	4
9.a	289·9	−0·5	10	52	−62·3	72	+ 24	11	3·5	20	8	490	2850	310	9	1·2	− 79	6
9.b	294·2	−1·1	11	33	−64·2	64	+ 21	6	3·5		8·5	520		330	9		−173	6
10.a	289·9	−2·7	10	52	−62·3	28	+ 84	15	3	14	12	730	3100	460	12·2	0·4	−589	4
10.b	296·2	−2·8	11	46	−64·2	28	+ 81	3	3·5		13·5	825		520	12	0·3	−611	4
11	304·0	−1·5	12	58	−64·1	56	+ 27	12	3	6·2	10·5	550	2850	400	9	1·0	−236	6
12.a	305·2	−2·0	13	12	−64·5	20	+ 84	6	4		15·5	1085		590	12·8	0·2	−436	4
12.b	308·2	−2·1	13	46	−64·0	20	+ 78	6	4	21	16	1120	6250	610	12·5	0·2	−458	4
12.c	315·9	−1·6	14	40	−61·4	20	+ 84	9	4		19	1330		730	14·2	0·2	−349	4
13.a	311·9	−0·7	14	06	−62·0	56	+ 36	12	3		12·5	650		480	9·5	0·9	−110	6
13.b	317·0	−1·1	14	50	−60·2	52	+ 36	15	[1·7]	32	14	[420]	7650	[540]	9·5	1·2	−173	6
13.c	324·4	−2·2	15	37	−56·1	48	+ 24	27	3		14·5	755		560	9	0·6	−345	6
14	325·5	−0·8	15	44	−56·4	32	+ 57	12	3	7·3	18	935	2300	690	12·1	0·3	−175	4
15.a	25·6	+0·1	18	35	− 6·5	36	− 30	12	4	13	19	1330	4300	730	12·2	0·3	+ 21	13
15.b	30·1	+0·2	18	43	− 2·4	36	− 39	15			19	1330		730	12·5	0·3	+ 42	13
16.a	40·1	+0·4	19	01	+ 6·4	44	− 45	27	4	20	16·5	1150	5600	630	11·7	0·4	+ 84	13
16.b	46·8	+0·8	19	12	+11·6	40	− 51	15			15·5	1080		630	11·5	0·4	+168	13
17.a	67·5	+0·8	19	56	+30·6	60	− 63	9	6·2	28	12	1070	5100	460	11·6	0·5	+168	13
17.b	76·5	+0·9	20	20	+38·2	56	− 75	15			10·8	1160		410	12	0·5	+189	13

TABLE 2 (*Continued*)

B. At Distances $R < R_0$

No.	l^{II} (deg)	b^{II} (deg)	α_{1960} h	α_{1960} m	δ_{1960} (deg)	$T_{max.}$ (°K)	r.v. (km/s)	$\Delta_{r.v.}$ (km/s)	Corrected Angular Dimensions b (deg)	Corrected Angular Dimensions l (deg)	r (kpc)	Linear Dimensions b (pc)	Linear Dimensions l (pc)	R (kpc)	$\bar{n}_H$ (H atoms cm^{-3})	Fig. No.
18	327·8	−0·4	15	51	−54·0	72	− 75	12	3	20	(1) 4·7	245	1650	5	2·9	9
											(2) 8·2	425	2850	4·7	1·7	
19	332·4	−0·1	16	13	−50·8	76	− 45	9	4	15	(1) 2·5	175	650	6	2·8	8
											(2) 10·3	720	2700	4·5	1·0	
20	341·2	−0·5	16	50	−44·6	32	−126	18	2·6	20	6	270	2100	3	1·2	10
21	353·3	−0·5	17	27	−34·8	20	− 87	27	2·6	11	5·2	234	1000	3	0·8	10
22.a	24·2	−0·4	18	34	− 8·0	52	+ 96	27	3	15	(1) 5·5	286	1450	4·1	1·6	11
22.b	30·4	−0·6	18	46	− 2·6	60	+ 78				(2) 10·0	520	2600	5	0·9	
23.a	35·9	−0·3	18	55	+ 2·5	60	+ 48	12	4	28	(1) 3·0	210	1450	6·3	4·3	12
23.b	48·4	−0·5	19	20	+13·5	92	+ 51	15			(2) 8·8	615	4300	6·3	1·5	
24.a	42·0	+2·2	18	58	+ 9·0	76	+ 33	12	9	20	(1) 2·2	345	750	6·5	2·1	14
24.b	47·5	+1·6	19	10	+13·6	76	+ 33				(2) 10·5	1650	3650	6·5	0·4	

listed in column 8 of Table 2, gives an indication of the velocity dispersion in a cloud. Values range from 3 to 27 km/s, with an average scatter for $R > R_0$ of 13 km/s. It is pointed out that McGee, Murray, and Pawsey (1961) found that in the motions of local hydrogen radial velocities ranged between ± 12 km/s and that ± 6 km/s were most representative.

The gas in our own local neighbourhood could well be considered to form one of the large clouds. The major components would be of the 100–150 parsec class, such as the Scorpius-Ophiuchus, Puppis-Vela, and Orion-Taurus-Perseus Clouds. Corresponding values to some of the Table 2 quantities would be $b \sim 250$ parsecs, l, say, ± 500 parsecs, and $\bar{n}_{\mathrm{H}}$ 0·5 H-atoms cm^{-3}.

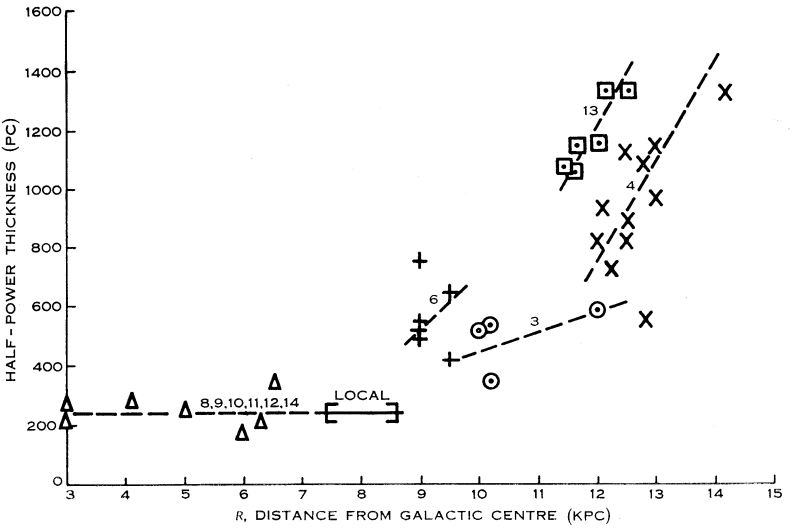

Fig. 16(*a*).—HI cloud thickness (at the half-power levels) plotted against distance from the galactic centre. Points marked △ are taken from Figures 8, 9, 10, 11, 12, 14; ⊙ from Figure 3; × from Figure 4; + from Figure 6; ⊡ from Figure 13. The heavy line in square brackets is the estimate for the solar neighbourhood.

(*b*) *HI Clouds at* $\mathrm{R} < \mathrm{R}_0$

Table 2B contains some limited information on 10 gas clouds inside the solar-galactic centre distance. It does not seem profitable to pursue it very far in view of the ambiguity in distance factor. If lower values of r, the distance from the Sun, are considered to apply in each case, the dimensions of thickness agree reasonably well with the previous work. The average z half-power thickness is 250 parsecs. The average velocity scatter $\overline{\triangle}_{\mathrm{r.v.}}$ is 16·5 km/s. The average mass of the clouds is $0{\cdot}4 \times 10^7 \mathrm{M}_{\odot}$.

If the positions were superimposed on Figure 15 the clouds could be said to correspond approximately to regions of increased density in the earlier diagram. However, if the greater r's be applied, a much better correspondence would seem to exist not only in position but also with the estimated densities, especially for the

spiral arms of Figures 11, 12, and 14. Enormous dimensions (the alternatives in Table 2B) must then be inferred for the clouds.

As mentioned earlier, some profile peaks become "lost" in the sides of wide profile components. Thus some clouds, especially at lower velocities, may not have been detected at all by the present method.

(c) *The Thickness and Density of HI Spiral Arms*

From the foregoing evidence and the general appearance of the $T_{\max.}$ contours we are led to the conclusion that the neutral hydrogen spiral arms are composed of these very large complexes or clouds. It is likely that the boundaries of adjacent clouds along an arm are intermixed, giving the effect of a background in the low level contours.

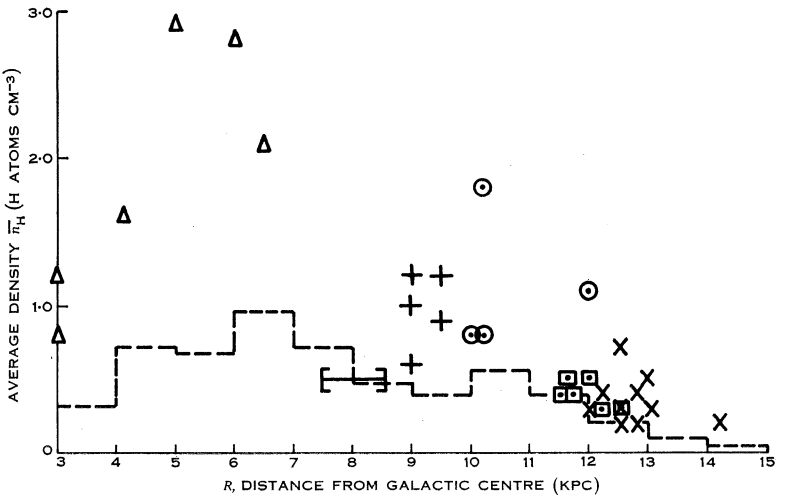

Fig. 16(*b*).—The estimated average density in the HI clouds plotted against distance from the galactic centre. The points are marked as in Figure 16(*a*). The dotted histogram is of Westerhout's (1957) densities calculated over annuli of 1 kpc in the galactic plane.

We collate some of the properties of the clouds by plotting the half-power thickness and the average density estimates against R, the distance from the galactic centre, in Figures 16(*a*) and 16(*b*). The points in the four outer arms have been given symbols characteristic of particular arms.

(i) *Thickness.*—In Figure 16(*a*) the points from $R = 3$ kpc to about $8 \cdot 5$ kpc are close to the 220 parsecs thickness (Schmidt 1957). At $R = 9$ kpc, an immediate increase in thickness begins and continuous to about 1300 parsecs at $R = 13$ kpc, the limit of the data. The points of the outer arms are so grouped that linear average curves may be drawn for each. These lines are labelled with the figure numbers of the corresponding contour diagrams.

Figure 16(*a*) shows us that the apparent thickness of the HI clouds and hence of the spiral arms increases markedly with distance from the galactic centre from $R \sim 9$ kpc.

This phenomenon has not received much attention in the literature. Van de Hulst, Muller, and Oort (1954), as a result of several cross-sectional sweeps through "a distant arm", found a "true half-thickness of 750 parsecs". Westerhout (1957) gives mean values of z up to 460 parsecs, which, however, he excluded from computations in determining a mean galactic plane. In discussing one of the "faint outer arms" he states that "its mean height between +500 and +1000 parsecs is very peculiar".

J. V. Hindman has informed us that he had noticed the great increase in the thickness of outer arms when investigating H-line data at Potts Hill, Sydney. An objection to the interpretation at the time was the possibility that the distribution was heliocentric and thus the apparent increase in thickness might be due to high velocity gas close to the Sun. However, on the present information given in Table 2, no heliocentric tendency is shown when the half-power thicknesses of the clouds are plotted against r, the distance from the Sun.

The large spread in the distribution of points of maximum hydrogen density in the diagram by Gum, Kerr, and Westerhout (1960) could well be due to the increasing thickness. For example, at 13 kpc the spread was approximately 800 parsecs.

(ii) *Density.*—The observed H-line brightness temperatures are found to decrease with R. From Table 2 we have:

$$\overline{T}_{\mathrm{b}} = 62^{\circ}\mathrm{K}, \qquad (R < R_0)$$
$$\overline{T}_{\mathrm{b}} = 44^{\circ}\mathrm{K}, \qquad (R > R_0)$$

for mean temperatures at the cloud maxima. An average value of 60°K at 9 kpc falls to $\sim$ 30°K at 13 kpc.

Since our estimates of $\bar{n}_{\mathrm{H}}$, the number of H-atoms per cm^3, are largely dependent on T_{b} (if the dimensions imposed by the model of Figure 15 be accepted) a similar decrease results in Figure 16(*b*). The dotted histogram represents Westerhout's (1957) calculations of densities of 1 kpc annuli. Our values are higher, as could be expected when the densities of concentrations of gas are compared with densities averaged over whole regions of the Galaxy.

For the outer arms, then, the thickness increases but the density decreases and, as stated in part (*a*) of this section, the masses of the contributing gas clouds remain fairly constant at about $10^7 \mathrm{M}_{\odot}$.

(*d*) *The HI Deficiencies in the Spiral Arms*

It could be suggested that the apparent boundaries of the HI clouds along the spiral arms might be, in fact, deficiencies in the emission caused by absorption of radiation from continuum radio sources lying in the same lines-of-sight.

In paper II, minima in the low velocity HI distribution along the galactic plane ridges, called col deficiencies, appeared to be due to absorption effects in some cases. Twenty examples of deficiencies occur in the $T_{\mathrm{max.}}$ diagrams of Figures 2 to 14(*a*), and examination has shown that in 12 of them col deficiencies (from paper II) do lie within a few degrees of the minimum values. No exact coincidence occurs and no real correspondence would be claimed. More importantly, no radio continuum sources have been reported close enough to the directions in question to warrant consideration.

V. The Radial Velocity Distribution

We have already made use of the distribution of radial velocity with galactic longitude to locate the spiral arms on the model in Section III. Two further aspects of the radial velocity information are now mentioned—the general shape and character of the contours seen in Figures 2 to 14(*b*) and the variation of radial velocity with galactic latitude.

(*a*) *The General Shape and Character of the Radial Velocity Contours*

The radial velocity contours tend to confirm the existence of the large-scale clouds of hydrogen we have proposed as the primary components of spiral arms. On inspection it can be seen that, as a rule, the velocity contours are fairly widely and evenly spread over the main body of a cloud as defined by the $T_{\text{max.}}$ contours but are bunched up into much stronger gradients in between clouds. Again, in the lower intensity levels towards the higher latitudes, increased velocity gradients are suggestive of cloud boundaries. Finally, in many cases rather marked velocity changes occur in the very low intensity levels; the contours are concentric about points situated at the very edges of the distributions. Thus, these velocity features seem to enclose areas corresponding to the shapes of the clouds as recognized from the companion $T_{\text{max.}}$ diagrams.

To illustrate the above we refer to Figure 3(*b*) where, in the region $l^{\text{II}} = 200°$ to 240°, the radial velocity contours are perpendicular to the galactic plane over the areas of Clouds 1 and 2. The contours become parallel to the plane with "foci" at $b^{\text{II}} = +17°$ and $-16°$, on a line almost exactly between the clouds.

The same effect can be noticed between Clouds 6 and 7 near $l^{\text{II}} = 250°$ to 280°. Increasing velocity gradients may be noticed to the north and at the high longitude end of Cloud 7.

In Figure 4(*b*) a stronger gradient exists between Clouds 3 and 4 ($l^{\text{II}} = 230°$ to 255°) than within them. The somewhat increased gradients parallel to the plane are present on both sides of Clouds 3, 4, and 5. Clouds 10*a* and 10*b* ($l^{\text{II}} = 285°$ to 302°) are separated by closed radial velocity contours.

Similar examples can be found in almost all the diagrams.

(*b*) *The Latitude Variation of Radial Velocity*

Kerr and Westerhout (1963) have referred to a linear velocity variation in galactic latitude over a limited portion of the "3½ kpc arm". The effect has been called a "rolling motion" of the arm. The magnitude is about 5 km s^{-1} deg^{-1}. The present radial velocity data is such that a general impression may be gained of velocity gradients over most of the observed gaseous spiral arms.

The radial velocity gradient with galactic latitude, $\Delta v/\Delta b$, has been measured at 10° intervals in galactic longitude on the diagrams 3 to 14(*b*). Regions of localized velocity changes, e.g. on the edges of clouds as mentioned in the previous subsection, have been avoided as far as possible. In determining gradients the radial velocity was plotted against b^{II} at the particular longitude and straight lines fitted between the points. Departures from linearity were low. In 18 of the 45 cases considered the

$\Delta v/\Delta b$ changed once, and usually in sign, in a central position of the arm; the five examples of two changes of gradient occurred only in the two outermost arms (Figs. 3 and 12(*b*)).

An attempt is made to summarize this data for the arms at $R > R_0$ in Figure 17 where $\Delta v/\Delta z$ is plotted against galactic longitude, l^{II}. The change has been made from b to z so that the distance factor may be taken into account. The units of $\Delta v/\Delta z$ are km s^{-1} (100 pc)$^{-1}$. The gradient has been called positive if the radial velocity increases positively as the latitude (or z) becomes more positive. The points from each spiral arm have their own symbols as in Figures 16(*a*) and 16(*b*). When two or three changes of gradient occur the points are marked 1, 2, 3 for successive values measured from the most negative latitudes. It will be seen that most of the gradients have quite low values, largely within ± 2 km s^{-1} (100 pc)$^{-1}$. The higher valued points at $l^{\mathrm{II}} = 240°$ to $270°$ from Figure 4(*b*) lie in the high gradient regions

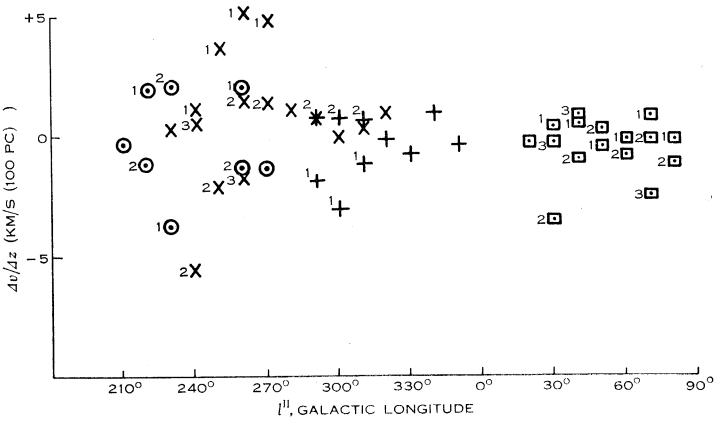

Fig. 17.—The gradient of radial velocity with the distance perpendicular to the galactic plane, plotted against galactic longitude. The points are again marked as in Figure 16,

mentioned in the example at the end of the previous subsection. The average of all the $\Delta v/\Delta b$ measured comes out at $+0\cdot 2$ km s^{-1} deg^{-1}. $\Delta v/\Delta z$ for the $3\frac{1}{2}$ kpc arm is approximately 5 km s^{-1} (100 pc)$^{-1}$ at $l^{\mathrm{II}} = 350°$ when calculated from Kerr's (1963) diagrams.

The points in $R < R_0$ would give a similar low-valued distribution for both possibilities of the distances ambiguity.

The results suggest that the "rolling motion" observed in the $3\frac{1}{2}$ kpc arm is unusual but that it does occur and over regions of greater dimensions in other spiral arms.

VI. Conclusion

The distributions of the intensity and the radial velocity of neutral hydrogen at other velocities than those previously treated in this series have been presented in a form close to the observational material. This is represented by the diagrams in Figures 1–14.

With an assumption about the relations between radial velocity and distance similar to that made by the earlier observers of HI spiral structure it is possible to show a general agreement with previous work. Distances and dimensions have been assigned to the various bodies of gas.

From the intensity diagrams it may be seen that the hydrogen occurs mainly in the form of large clouds of much greater dimensions than have previously been reported; the clouds appear to be the principal elements of the gaseous spiral arms.

Although the possible thickness of the galactic HI layer in the regions $R < R_0$ agrees with the value found by previous workers, we find that in $R > R_0$, where four spiral arms can be traced, the thickness increases with increasing distance from the galactic centre. At $R = 13$ kpc the half-power thickness is estimated to be 1300 parsecs.

The gas density also decreases with R in such a way that the estimated masses of the large clouds are found to remain at a value of $10^7 M_\odot$ throughout the Galaxy. The mass compares with the value $2 \times 10^7 M_\odot$ average found by the authors (McGee and Milton 1963) for individual HI clouds in the outer regions of the Large Cloud of Magellan.

The radial velocity distribution supports the evidence from the intensity distribution of the reality of the large gas clouds.

VII. Acknowledgment

The authors are grateful to Miss Wendy Wolfe for her assistance in the reduction of observations and the preparation of some of the diagrams.

VIII. References

Blaauw, A., Gum, C. S., Kerr, F. J., Oort, J. H., Pawsey, J. L., Rougoor, G. W., and Westerhout, G. (1960).—New IAU System of Galactic Coordinates (1958 Revision). *Mon. Not. R. Astr. Soc.* **121**: 123–73.

Bracewell, R. N., and Roberts, J. A. (1954).—*Aust. J. Phys.* **7**: 615–40.

Gum, C. S., Kerr, F. J., and Westerhout, G. (1960).—*Mon. Not. R. Astr. Soc.* **121**: 132–49.

van de Hulst, H. C. (1958).—*Rev. Mod. Phys.* **30**: 913–23.

van de Hulst, H. C., Muller, C. A., and Oort, J. H. (1954).—*Bull. Astr. Insts. Netherlds.* **12**: 117–49.

Kerr, F. J. (1962).—*Mon. Not. R. Astr. Soc.* **123**: 327–45.

Kerr, F. J. (1963).—IAU Symposium No. 20 (in press.)

Kerr, F. J., Hindman, J. V., and Gum, C. S. (1959).—*Aust. J. Phys.* **12**: 270–92.

Kerr, F. J., and Westerhout, G. (1963).—"Compendium on Stars and Stellar Systems." Vol. 5. (in press.)

McGee, R. X. (1963).—IAU Symposium No. 20 (in press.)

McGee, R. X., and Milton, Janice A. (1963).—I.A.U. Symposium No. 20 (in press.)

McGee, R. X., and Murray, J. D. (1961).—*Aust. J. Phys.* **14**: 260–78.

McGee, R. X., and Murray, J. D. (1963).—*Proc. Instn. Radio Engrs. Aust.* **24**: 191–6.

McGee, R. X., Murray, J. D., and Milton, Janice A. (1963).—*Aust. J. Phys.* **16**: 136–70.

McGee, R. X., Murray, J. D., and Pawsey, J. L. (1961).—*Nature* **189**: 957–9.

MacRae, D. A., and Westerhout, G. (1956).—Tables for the reduction of velocities to the local standard of rest. The Observatory, Lund, Sweden.

Muller, C. A., and Westerhout, G. (1957).—*Bull. Astr. Inst. Netherlds.* **13**: 151–95.

Ollongren, A., and van de Hulst, H. C. (1957).—*Bull. Astr. Inst. Netherlds.* **13**: 196–200.

Schmidt, M. (1957).—*Bull. Astr. Inst. Netherlds.* **13**: 247–68.

Westerhout, G. (1957).—*Bull. Astr. Inst. Netherlds.* **13**: 201–46.